Pergamon

Scripta Materialia, Vol. 40, No. 2, pp. 191–196, 1999
Published by Elsevier Science Ltd

1359-6462/99 $0.00 + .00

PII S1359-6462(98)00406-0

MICROSTRUCTURES AND MECHANICAL PROPERTIES OF A Mo_3Si-Mo_5Si_3 COMPOSITE

A. Misra, J. J. Petrovic and T. E. Mitchell
Materials Science and Technology Division, Los Alamos National Laboratory, MS K765, Los Alamos, NM 87545

(Received September 30, 1998)
(Accepted October 9, 1998)

Introduction

The silicide intermetallic compounds in the Mo-Si system are of interest as high temperature structural materials (1–3). While most of the early work focussed on $MoSi_2$ and its composites with ceramic reinforcements such as SiC, TiC and ZrO_2 (1,3), some recent studies indicate boron-doped Mo_5Si_3 as a promising creep resistant material with good oxidation resistance (4,5). Further, $MoSi_2$-Mo_5Si_3 eutectic composites have superior creep resistance as compared to monolithic $MoSi_2$ in the temperature range of 1100–1400°C (6). Unfortunately, monolithic $MoSi_2$ and Mo_5Si_3 as well as $MoSi_2$-Mo_5Si_3 composites all have very low fracture toughness at room temperature. Experiments on Mo-Si diffusion couples have suggested that cracks in the Mo_5Si_3 and $MoSi_2$ phases formed due to thermal stresses may have been blunted by the Mo_3Si layer (7). A detailed investigation of the mechanical properties of Mo_3Si may help in the development of Mo_3Si-Mo_5Si_3 or Mo-Mo_3Si *in situ* composites.

Mo_3Si has the cubic A15 structure (β-W or Cr_3Si type) where the Si atoms occupy the bcc positions in the unit cell and the Mo atoms form three orthogonal chains along the ⟨100⟩ directions on the cube faces, as shown schematically in Fig. 1 (8). Unlike $MoSi_2$ and Mo_5Si_3 which melt congruently at 2020°C and 2180°C respectively, Mo_3Si forms through a peritectic reaction, L + (Mo) $\Rightarrow$ Mo_3Si at 2025°C (9). The Mo_3Si-Mo_5Si_3 eutectic is reported to occur at 2020°C at a composition of 26.4 at.% Si (9). While the mechanical properties of A15 compounds such as Nb_3Al, Cr_3Si and V_3Si have been investigated (10), no literature exists on the mechanical properties of Mo_3Si. A comparison of some physical properties of these A15 compounds is shown in Table 1 (8–14). Note that Mo_3Si has a relatively high melting point (reported here as the peritectic temperature) but also has a higher density than the other A15 compounds listed in Table 1. The ductile-to-brittle transition temperatures (DBTT) of Nb_3Al, Cr_3Si and V_3Si have been found to be greater than 1200°C (10). The slip systems of A15 compounds such as Nb_3Al (11), Cr_3Si (12) and V_3Si (13) are reported to be {100}⟨010⟩ and so the lattice parameters listed in Table 1 are also the magnitudes of the respective Burgers vectors. As expected, both Nb_3Al and V_3Si were found to have poor oxidation resistance (10). Cr_3Si was also found to have inadequate oxidation resistance above 1200°C due to the preferred formation of Cr_2O_3 over SiO_2 (14). However, excellent oxidation resistance was observed in ternary $(Cr,Mo)_3Si$ alloys (14) suggesting that Mo_3Si may have good oxidation resistance. In this investigation, the microstructures and mechanical properties of a solidification processed Mo_3Si-Mo_5Si_3 composite are reported.

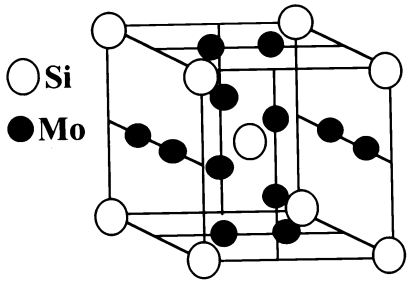

Figure 1. A15 unit cell of Mo_3Si.

Experimental Procedures

Mo_3Si-Mo_5Si_3 alloys were prepared by arc-melting pure Mo and Si, using ~1 at.% excess Si beyond the eutectic composition in the initial melting charge to compensate for Si loss during melting. The arc-melted buttons were remelted together in a cigar-shaped hearth to prepare the feed rod for single crystal growth by optical floating-zone melting. The arc-melted feed rod was given a float-zone pass at ~15 mm/hour. Powder X-ray diffraction was performed to identify the phases present in the solidification processed alloy. The mechanical properties were evaluated by hot hardness experiments using a Vickers indentor at 1kg load in the temperature range of 25–1300°C using a Nikon QM2 instrument. Scanning electron microscopy (SEM) was performed on a JEOL 6300FXV microscope operating at 15 kV and transmission electron microscopy (TEM) was performed on a Philips CM30 microscope operating at 300 kV.

Results and Discussion

All results presented are from the float-zone processed rods. Powder X-ray diffraction indicated that the alloys contain only two phases, Mo_3Si and Mo_5Si_3. The microstructure, viewed normal to the solidification direction, is shown in Fig. 2. The Mo_3Si-Mo_5Si_3 eutectic regions as well as pro-eutectic Mo_5Si_3 phase are observed. This indicates that the overall composition of the alloy is slightly higher than the eutectic composition, 26.4 at.% Si. Within the eutectic regions, the measured volume fraction of the Mo_5Si_3 phase was 12 ± 1%, very close to the 11.67% calculated from the phase diagram. The Mo_5Si_3 precipitates were ~8–10 μm in diameter with an inter-particle spacing of 15–20 μm.

TEM was used to characterize the Mo_3Si-Mo_5Si_3 orientation relationship, as well as interfaces and defects in the as-processed alloy. Since Mo_5Si_3 is tetragonal with lattice parameters of a= 9.64 A° and c= 4.91 A° (15) compared to a= 4.89 A° for cubic Mo_3Si (8), it follows that c(Mo_5Si_3) ≈ a(Mo_3Si),

TABLE 1
Comparison of Some Physical Properties of Selected A15 Compounds

Alloy	Melting Point (°C)	Density (g/cm^3)	Lattice Constant (A°)
Nb_3Al	2060	7.3	5.19
Cr_3Si	1770	6.5	4.56
V_3Si	1925	5.7	4.71
Mo_3Si	2025	8.9	4.89

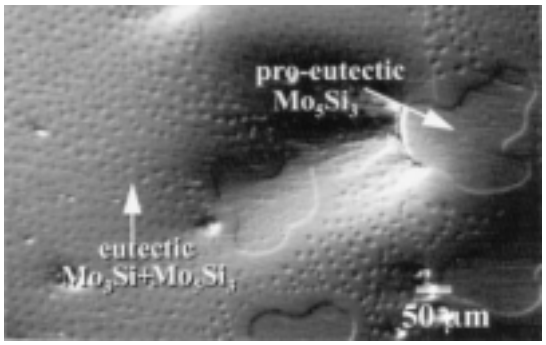

Figure 2. Light micrograph showing the transverse section of the microstructure of float-zone processed Mo_3Si-Mo_5Si_3 alloys.

and a/2(Mo_5Si_3) ≈ a(Mo_3Si). Thus, the simplest orientation relationship expected would be that the c-planes of Mo_5Si_3 are parallel to cube planes of Mo_3Si and the a-axis of Mo_5Si_3 is parallel to a cube axis of Mo_3Si. In the few precipitates examined, this simple orientation relationship was in fact not observed. [111] Mo_3Si was found to be within 2° of [113] Mo_5Si_3 and (110) Mo_3Si was misoriented by ~7° from (110)Mo_5Si_3. The stereographic projection of this relationship indicated that [100] Mo_3Si was misoriented by ~7° from [100] Mo_5Si_3. No misfit dislocations were resolved at the Mo_3Si-Mo_5Si_3 interface with bright field imaging. A more detailed study of the interface structure and crystallography is needed to understand the misfit accommodation at the interface and the reasons for misorientation between the low index directions.

TEM foils also exhibited fine cracks in the Mo_3Si phase almost parallel to, but away from, the interface as shown in Fig. 3(a). Dislocations were observed in the Mo_3Si phase at the tip of these cracks in the TEM foils from as-float zone processed samples (Fig. 3(b)). Other regions and the Mo_5Si_3 precipitates were usually dislocation-free. These dislocations were analyzed to be of the {100}⟨010⟩ type, consistent with the reports on other A15 compounds (11–13). No other slip systems were observed.

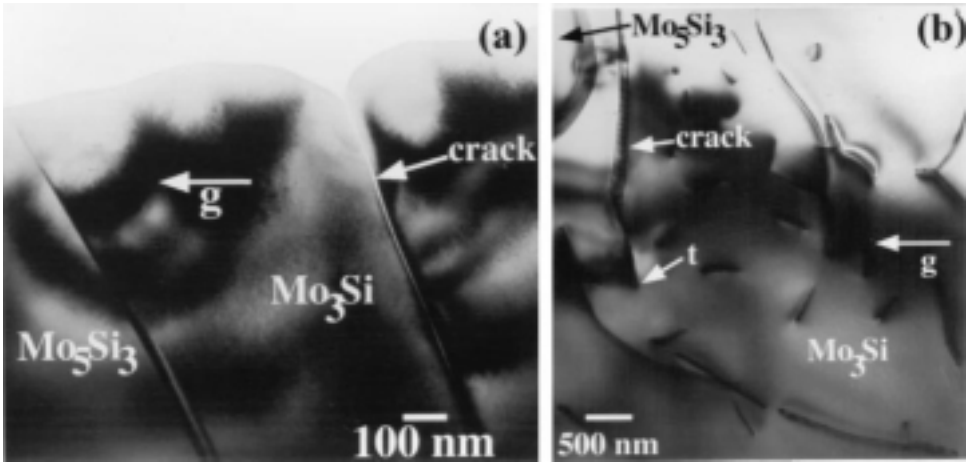

Figure 3. Bright field TEM images showing (a) a crack in the Mo_3Si phase away from the interface and (b) dislocations near the crack tip (marked by an arrow and labeled "t"). These dislocations were identified to be of the {100}⟨010⟩ type. **B** = [001] and **g** = 120 in both.

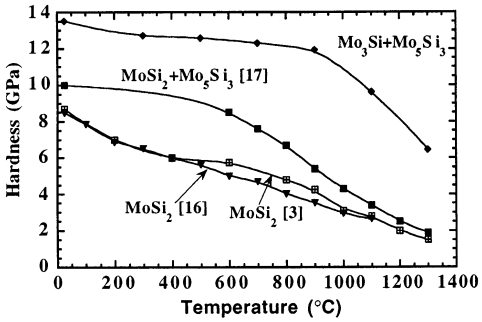

Figure 4. Hot hardness of the Mo_3Si-Mo_5Si_3 *in situ* composites. Data from literature on arc-melted $MoSi_2$-Mo_5Si_3 composites (17), arc-melted $MoSi_2$ (3) and hot-pressed $MoSi_2$ (16) are also shown for comparison.

Mechanical properties were evaluated by hot hardness indentations and the results are shown in Fig. 4. For comparison, hot hardness data on hot-pressed $MoSi_2$ from Maloy et al. (16), arc-melted $MoSi_2$ from Gibala et al. (3), and arc-melted $MoSi_2$-Mo_5Si_3 eutectic composites ($\sim$45 vol.% of Mo_5Si_3) from Mason and Van Aken (17) are also shown in Fig. 4. The room temperature hardnesses of Mo_3Si and Mo_5Si_3 have been reported as 12.85 GPa and 11.48 GPa respectively (18), using which a rule-of-mixtures value for the $MoSi_2$-Mo_5Si_3 eutectic was obtained as $\sim$12.7 GPa, roughly consistent with the 13.5 GPa hardness measured in this investigation. Note that at room temperature the hardness of Mo_3Si-Mo_5Si_3 composites is $\sim$35% higher than $MoSi_2$-Mo_5Si_3 eutectic composites and $\sim$60% higher than that of monolithic $MoSi_2$. It should be pointed out that the $MoSi_2$-Mo_5Si_3 composites had fine microstructures with eutectic spacing on the order of 1 μm (17), about an order of magnitude lower than the microstructural scale of Mo_3Si-Mo_5Si_3 composites evaluated in this investigation. The hardness of Mo_3Si-Mo_5Si_3 alloys is fairly constant till about 900°C and then gradually decreases with increasing temperature but is still $\sim$6 GPa at 1300°C. On the other hand, the $MoSi_2$-Mo_5Si_3 composites show a more rapid decrease in hardness with increasing temperature and have about the same hardness as $MoSi_2$ at 1300°C, which is a factor of 3 lower than that of Mo_3Si-Mo_5Si_3 composites. Thus, it can be inferred that the high hardness and excellent hardness retention of Mo_3Si-Mo_5Si_3 composites with increasing temperature is primarily due to the intrinsic properties of Mo_3Si and cannot be attributed solely to possible strengthening from the Mo_5Si_3 phase (volume fraction $\approx$ 0.12).

Indentation toughness (K_c) was determined by measuring the lengths of the radial cracks emanating from the Vickers indents, using the following relation from (19):

$$K_c = A(E/H)^{1/2}(P/c^{3/2})$$

where A is a constant of value 0.016 (19), E is the Young's modulus, H is the hardness, P is the load and c is the half-crack length. E for Mo_3Si is reported as 295 GPa (18) and for Mo_5Si_3 as $\sim$260 GPa (20). Using these literature values, the Young's modulus of Mo_3Si-Mo_5Si_3 eutectic composite was estimated by rule-of-mixtures as 290 GPa. The average K_c values of Mo_3Si-Mo_5Si_3 composites as a function of temperature are shown in Fig. 5. Up to 1100°C, the toughness is roughly constant in the range of 1.5–2 MPa$\sqrt{}$m. A rapid increase in K_c is observed in the range of 1100°C to 1300°C. The data at 1300°C are lower-bound estimates since radial cracks were observed to emanate only from two corners of the indents and not all four. No indication of room temperature plasticity around indents was discerned as shown in Fig. 6. Indents like the one shown in Fig. 6 were not used to measure c for estimation of K_c since multiple cracks, including lateral cracks, were observed. Some evidence of crack deflection along the Mo_3Si-Mo_5Si_3 interface (marked as "I" in Fig. 6) and of the fracture of the Mo_5Si_3

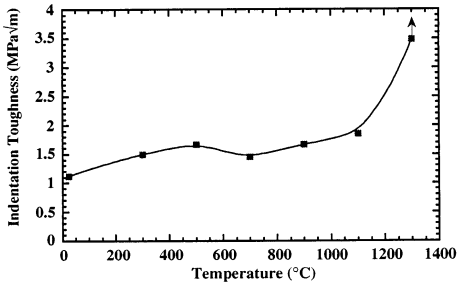

Figure 5. Indentation toughness of the Mo_3Si-Mo_5Si_3 *in situ* composites as a function of temperature.

precipitates (marked as "f" in Fig. 6) is observed. However, Mo_5Si_3 does not appear to act as a toughening phase for Mo_3Si.

The key to understanding the high strength of Mo_3Si is in its A15 structure. The Mo atoms form three mutually perpendicular chains along the cube directions with a nearest-neighbor spacing between atoms of a/2 (where a is the lattice parameter). This may indicate a very strong directional bonding along the chains. Therefore, the easiest slip systems to operate are the {100}⟨010⟩ type. However, as shown in Table 1 the magnitude of the ⟨100⟩ Burgers vector is large and would result in a high Peierls stress. Dissociation of the as-grown ⟨100⟩ dislocations was not observed but has been reported in deformed specimens of other A15 compounds, e.g. Nb_3Al (11). Other slip vectors, such as the ⟨110⟩ or ⟨111⟩ type, would require breaking the Mo-Mo chains and hence, will have much higher critical resolved shear stress. Since {100}⟨010⟩ only gives 3 independent slip systems, polycrystalline ductility is not possible in A15 compounds. In this investigation, compressive deformation of single crystalline Mo_3Si has not been performed to evaluate the slip systems as a function of temperature. Such studies have been performed on other A15 compounds such as Nb_3Al (11), Cr_3Si (12) and V_3Si (13) and only the {100}⟨010⟩ slip system has been reported. In Cr_3Si (12), polycrystalline ductility, in compression, was

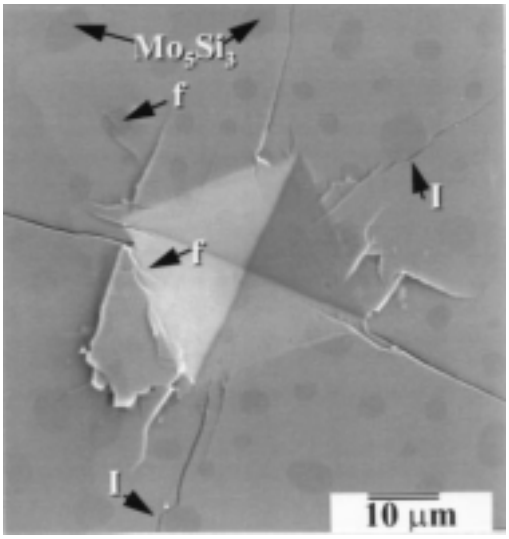

Figure 6. SEM micrograph showing a room temperature hardness indent in the Mo_3Si-Mo_5Si_3 *in situ* composite. Crack deflection along the interface (marked "I") and fracture of Mo_5Si_3 precipitates (marked "f") are observed. No evidence of plasticity around the indents is seen.

not observed below 1350°C, whereas single crystals could only be deformed above 1200°C. Even at 1350°C, only the {100}⟨010⟩ slip system was observed in single crystals of Cr_3Si (12). In V_3Si compressed at 1600°C, in addition to the observation of a few isolated screw dislocations on {100}⟨010⟩, both twist and tilt sub-boundaries were also observed indicating recovery and climb (13). Thus, the inherent brittleness of Mo_3Si may be related to its A15 structure. Better combination of high temperature strength and room temperature toughness may be achieved in two-phase Mo-Mo_3Si alloys and this will be the subject of future work.

Summary and Conclusions

Float-zone processed Si-rich Mo_3Si alloys exhibited a two-phase microstructure having pro-eutectic Mo_5Si_3 and eutectic Mo_3Si-Mo_5Si_3. These alloys exhibit very high hardness and excellent hardness retention with increasing temperature. Even at 1300°C, the hardness was about a factor of 3 higher than that of $MoSi_2$-Mo_5Si_3 eutectic composites. The indentation toughness was <2 MPa$\sqrt{m}$ up to 1100°C but increased to $\sim$3.5 MPa$\sqrt{m}$ at 1300°C. TEM investigation of the dislocations in the as-cast alloys revealed only the {100}⟨010⟩ slip system. More work is needed to characterize the deformation behavior of single crystal Mo_3Si and the two-phase Mo-Mo_3Si alloys to better evaluate the potential of Mo_3Si-based alloys for high temperature structural applications. These studies are currently underway.

Acknowledgements

This research is sponsored by DOE, Office of Basic Energy Sciences. The assistance of Mr. Richard C. Hoover, Los Alamos National Laboratory, is acknowledged.

References

1. J. J. Petrovic, Ceram. Eng. Sci. Proc. 18, 3 (1997).
2. T. E. Mitchell, R. G. Castro, J. J. Petrovic, S. A. Maloy, O. Unal, and M. M. Chadwick, Mater. Sci. Eng. A155, 241 (1992).
3. R. Gibala, A. K. Ghosh, D. C. Van Aken, D. J. Srolovitz, A. Basu, H. Chang, D. P. Mason, and W. Yang, Mater. Sci. Eng. A155, 147 (1992).
4. M. K. Meyer and M. Akinc, J. Am. Ceram. Soc. 79, 938 (1996).
5. M. K. Meyer, M. J. Kramer, and M. Akinc, Intermetallics 4, 273 (1996).
6. D. P. Mason and D. C. Van Aken, Acta Metall. Mater. 43, 1201 (1995).
7. P. C. Tortorici and M. A. Dayananda, Mater. Sci. Eng. A, to be published.
8. J. H. Westbrook, Intermetallic Compounds, John Wiley & Sons, Inc., New York (1967).
9. A. B. Gokhale and G. J. Abbaschian, Binary Alloy Phase Diagrams, ASM Int., Metals Park, OH (1990).
10. D. M. Shah and D. L. Anton, Mater. Sci. Eng. A153, 402 (1992).
11. T. N. Marieb, A. D. Kaiser, S. R. Nutt, D. L. Anton, and D. M. Shah, Mater. Res. Symp. Proc. 213, 329 (1991).
12. C. S. Chang and D. P. Pope, Mater. Res. Symp. Proc. 213, 745 (1991).
13. L. S. Smith, M. Aindow, and M. H. Loretto, Mater. Res. Symp. Proc. 288, 477 (1993).
14. S. V. Raj, Mater. Sci. Eng. A201, 229 (1995).
15. S. V. N. Naidu, C. F. Mays, and C. R. Houska, Commun. Am. Ceram. Soc. C-58, April (1982).
16. S. A. Maloy, A. H. Heuer, J. J. Lewandowski, and J. J. Petrovic, J. Am. Ceram. Soc. 74, 2704 (1991).
17. D. P. Mason and D. C. Van Aken, Scripta Metall. Mater. 28, 185 (1993).
18. G. V. Samsonov and I. M. Vinitskii, Handbook of Refractory Compounds, pp. 287–297, IFI/Plenum Company, New York (1980).
19. G. R. Anstis, P. Chantikul, B. R. Lawn and D. B. Marshall, J. Am. Ceram. Soc. 64, 533 (1981).
20. S. R. Srinivasan and R. B. Schwarz, J. Mater. Res. 7, 1610 (1992).